RSC Advances

PAPER

View Article Online
View Journal | View Issue

Cite this: *RSC Adv.*, 2023, **13**, 2392

Sensitive detection of 4-nitrophenol based on pyridine diketopyrrolopyrrole-functionalized graphene oxide direct electrochemical sensor†

Lingpu Jia, *[a] Juan Hao,[b] Shuangshuang Wang,[c] Long Yang [c] and Kunping Liu [b]

Received 15th November 2022
Accepted 7th December 2022

DOI: 10.1039/d2ra07239d

rsc.li/rsc-advances

For highly sensitive detection of 4-nitrophenol (4-NP) in the environment, a novel pyridine diketopyrrolopyrrole-functionalized graphene oxide (PDPP–GO) composite was constructed for the first time by an improved Hummers' method. Herein, PDPP was completely dissolved in sulfuric acid (6 mol L^{-1}) and reacted with GO, promoting PDPP evenly adhering to the GO surface. Moreover, the specific surface area increased from 15.51 to 22.033 m^2 g^{-1}. Infrared spectroscopy and X-ray photoelectron spectroscopy simultaneously demonstrated that PDPP was bound to GO by the strong intermolecular hydrogen bonding and π–π stacking conjugation. During the cyclic voltammetry test, the PDPP–GO coated glassy carbon electrode (PDPP–GO/GCE) direct electrochemical sensor gave expression to the best electrocatalytic activity for 4-nitrophenol detection than GO/GCE and bare GCE. Under optimization conditions, the as-prepared PDPP–GO/GCE sensor brought out remarkable sensitivities of 18.54 (0.5–50 μM) and 6.61 μA μM^{-1} cm^{-2} (50–163 μM) in the linear detection of 4-NP. Besides, a low detection limit of 0.10 μM, reliable long-term stability, excellent selectivity, and reproducibility were obtained. In the real sample test, the PDPP–GO/GCE demonstrated sensitive and reliable determination.

1. Introduction

4-Nitrophenol (4-NP) as an important raw material is widely used to synthesize medicines, pesticides, and dyes.[1,2] However, typically, the toxicity of 4-NP can cause cancer, deformity and is mutation-carcinogenic for humans and animals.[3–5] Therefore, it is very important to monitor 4-NP at low concentrations during environmental analysis. Besides, the Soviet Union stipulates that the initial safe level of surface water is 0.02 mg L^{-1}. To date, many efficient methods have been developed to supervise 4-NP, such as high-performance liquid chromatography,[6] fluorescence measurement,[7] gas chromatography-mass spectrometry, gas chromatography,[8,9] capillary electrophoresis, photoelectrochemical,[10] and electrochemical methods.[11,12] Among these methods, the electrochemical methods are often preferred by researchers for merits of sensitivity, selectivity, rapid response time, simple operation, and being environment-friendly.

For the electrochemical method, the comprehensive performance of the electrochemical sensor depends on the surface property and composition of modified materials, and thus endless new materials are being synthesized and used to detect objects.[13,14] Using 4-NP as the target, various composite materials based on metals, metals oxides, carbon nanomaterials, metal–organic frameworks, and organics have been studied with satisfactory results.[15–17] However, the fabrication of a simple, highly sensitive, stable electrochemical sensor is always a great challenge at low cost. Thus far, graphene-based materials with novel physical and chemical properties have become a preferred partner of modified electrodes.[18] Graphene oxide (GO) possesses abundant polar functional groups with hydroxyl, carboxyl, and epoxy bonds, which offer opportunities for modification and hybridization with other materials,[19] but it is well known that the non-conductive GO is against the electrocatalytic reaction.

Pyridine diketopyrrolopyrrole (PDPP) belongs to diketopyrrolopyrrole (DPP) conjugated polymers with central symmetry. As an electron-deficient system, DPP has a conjugated planar backbone, which results in strong π–π stacking interactions. Moreover, DPP conjugated polymers show ultra-high corrosion resistance, good photoelectric properties,[20]

[a]*Key Laboratory of Medicinal and Edible Plants Resources Development of Sichuan Education Department, Institute for Advanced Study, Chengdu University, Chengdu 610106, China. E-mail: jialingpu@cdu.edu.cn*

[b]*Key Laboratory of Medicinal and Edible Plants Resources Development of Sichuan Education Department, Sichuan Industrial Institute of Antibiotics, School of Pharmacy, Chengdu University, Chengdu 610106, China*

[c]*State Key Laboratory of Environment-Friendly Energy Materials, School of Materials Science and Engineering, Southwest University of Science and Technology, Mianyang 621010, China*

† Electronic supplementary information (ESI) available. See DOI: https://doi.org/10.1039/d2ra07239d

high-charge carrier mobility,[21] excellent crystallinity[22] and are environment-friendly and exhibit promising potential in organic field-effect transistors and polymer solar cells.[23–25] In organic systems, PDPP and other DPP-conjugated polymers have been extensively investigated.[26–28] However, because of the limitation of non-modification PDPP that can be dissolved in sulfuric acid ($C \geq 6$ mol L^{-1}) only, relevant studies in aqueous solution have not been reported. Compared with the DPP ring, the planar conjugated bicyclic structure and secondary amino of PDPP can also prompt the formation of strong π–π interaction, chemical bond, and intermolecular hydrogen bonding with others;[29] thus, it is expected to combine with two-dimensional nanomaterials and develop into a new field.

In order to fabricate a simple rapid electrochemical sensor with highly sensitive and long-stable based on GO, the organic semiconductor material PDPP was used to change the electronic structure and surface properties of GO. During the preparation process of GO with the Hummers' method, the whole system involves a concentrated sulfuric acid system, which provides a good solvent condition for PDPP. Therefore, we attempted to synthesize PDPP–GO composite material in the above suitable solvent environment. After a survey on the molecular structure of PDPP and GO, the amine bond of PDPP may react with the hydroxyl and carboxyl bonds of GO by chemical bonding, hydrogen bonding, or intermolecular forces.[30] Furthermore, the introduction of PDPP could bring new opportunities for the development of GO or PDPP-based composite materials.

In this work, PDPP–GO composite material was first synthesized in an aqueous solution and PDPP–GO modified glassy carbon electrode (PDPP–GO/GCE) showed excellent electrocatalytic activity for 4-NP detection. The interactions between the PDPP and GO molecules were fully analysed by infrared spectroscopy and X-ray photoelectron spectroscopy, and PDPP tightly combined with the GO by strong hydrogen bonding and π–π stacking conjugation. The comprehensive sensing performances of PDPP–GO/GCE with excellent sensitivity, selectivity, stability, and reproducibility perfectly meet the requirements for modern electrochemical sensors.

2. Materials and methods

2.1 Materials and instrumentation

Graphite powder was purchased from Xiya Chemical Technology (Shandong) Co., Ltd. Sodium nitrate ($NaNO_3$), potassium permanganate ($KMnO_4$), dipotassium hydrogen phosphate (K_2HPO_4), and potassium dihydrogen phosphate (KH_2PO_4) were received by Chengdu joint chemical reagent research institute (Sichuan). Concentrated sulfuric acid (H_2SO_4) and hydrogen peroxide (30% H_2O_2) were obtained from Chengdu Kelong Chemical Reagent Factory (Sichuan). Pyridine-diketopyrrolopyrrole (PDPP) was obtained from the laboratory of Chengdu Zhongjin Pharmaceutical Technology Co., Ltd. Other reagents used for the interference determination were all analytically pure. All the aqueous solutions were prepared with deionized water.

The surface morphology was observed using a field-emission scanning electron microscope (FE-SEM) (Carl Zeiss SMT Pte Ltd., Germany). X-ray diffraction (XRD) (D/max-r A type Cu Kα, 3–80°) and X-ray photoelectron spectroscopy (XPS) were used for studying the crystalline structures and chemical environment of elements, respectively. Fourier transformation infrared spectroscopy (FT-IR) data were collected using an FT-IR spectrometer (Spectrum one, America). A specific surface area and pore size analyzer (Autosorb-IQ, N2, Quantachrome Instruments) was used for measuring the special surface area of samples. All electrochemical experiments were carried out on the CHI 630E workstation (CH Instrument, USA) with a three-electrode system, in which PDPP–GO-modified glassy carbon electrode (GCE) acted as the working electrode, standard calomel electrode $Hg/HgCl_2$ and platinum wire played roles of the reference and the auxiliary electrode, respectively.

2.2 Synthesis of PDPP–GO composite materials

PDPP–GO composite material was synthesized by the improved Hummers' method.[31] First, 0.0500 g PDPP was dissolved in 30.0 mL concentrated H_2SO_4 in a beaker. Then, 0.5000 g graphite, 0.2500 g $NaNO_3$, and 1.5000 g $KMnO_4$ were added to the above solution and stirred for 12 h at room temperature. Thereafter, the solution was diluted with 50.0 mL of distilled water by keeping the temperature below 20 °C, and then 2.5 mL H_2O_2 (30%) and 100.0 mL of distilled water were added to the suspension, constantly stirred and sonicated for 6 h at 60 °C. In order to remove the uncompounded PDPP, the obtained solid was washed with sulfuric acid (6 mol L^{-1}), and then dealt with deionized water until the pH value reached 7. Finally, the obtained PDPP–GO composite was dried at 60 °C for 12 h. The other mass ratios of PDPP–GO (wt%: 15%, 20%, 25%, 30%) and GO were also obtained by the same method. The 25% PDPP–GO sample was denoted as PDPP–GO.

2.3 Preparation of PDPP–GO/GCE

Before use, GCE was polished carefully with 0.3 mm alumina and washed thoroughly with deionized water and ethanol. Then 10.0 μL different ratios of PDPP–GO (1.0 mg mL^{-1}) dispersion in deionized water were dropped on the surface of GCE, and the prepared electrode was labelled as PDPP–GO/GCE. Before the electrochemical test, the electrolytic solution was fed with nitrogen for 10 minutes to remove oxygen. The synthetic processes of PDPP–GO/GCE are shown in Scheme 1.

The electrode surface area of PDPP–GO/GCE was analyzed by cyclic voltammetric technique with 1.0 mM $K_3Fe(CN)_6$ as a probe at various scan rates in 0.1 M KCl. For a reversible electrode process ($T = 298$ K), the Randles–Sevcik equation is as follows:

$$i_{pa} = 0.4463(F^3/RT)^{1/2} n^{3/2} A_0 D_0^{1/2} v^{1/2} C_0 \quad (1)$$

where i_{pa} is the anodic peak current, and the n, A_0, D_0, C_0, and v, respectively, represent the number of electrons transferred, surface area, diffusion coefficient, concentration, and scan rate of $K_3Fe(CN)_6$. Meanwhile, for 1.0 mM $K_3Fe(CN)_6$ in 0.1 M KCl

Scheme 1 The synthetic processes of PDPP–GO/GCE.

electrolyte, $F = 96\,485$ C mol^{-1}, $R = 8.314$ J K^{-1} mol^{-1}, $T = 298$ K, $n = 1$, and $D_0 = 7.6 \times 10^{-6}$ cm^2 s^{-1}. Hence, the A_0 can be obtained from the slope of the plot of i_{pa} *vs.* $v^{1/2}$.[32,33] At last, the A_0 of GCE and PDPP–GO/GCE were found to be 0.0406 and 0.1749 cm^2, respectively.

3. Results and discussion

3.1 Characterization of PDPP–GO composite material

FT-IR spectroscopy was chosen to probe the reaction mechanism and structure of PDPP–GO composite material. Fig. 1 shows the FT-IR spectra of PDPP, GO, and PDPP–GO. These peaks appeared at 3130–3430, 2700–3050, 1730, and 1651 cm^{-1}, corresponding to the stretching vibrations of –NH, –CH=CH, C=O, and C=C, respectively.[26] In the curve of GO, the stretching vibration peaks of –OH, –CH=CH–, C=O, and C=C are displayed at 3430, 2820–3000, 1729, and 1625 cm^{-1}, respectively.[34] By analysing the obtained curves shown in the figure, what is notable is that the –CH=CH at 2830–2930 cm^{-1} of PDPP–GO has a red-shift and blue-shift compared with GO and PDPP, respectively, and the C=O (1725 cm^{-1}) characteristic peak remains unchanged compared with GO. These results indicate that π–π stacking interactions or hydrogen bond exit in the PDPP–GO, which push the electron cloud of PDPP towards GO.

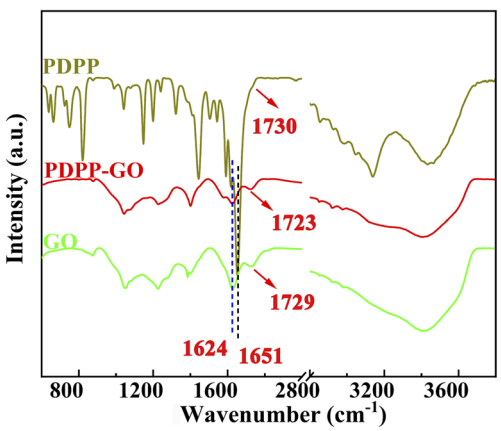

Fig. 1 FT-IR spectra of PDPP, GO, and PDPP–GO.

Scanning electron microscopy was utilized to reveal the morphologies of the target materials. The rice-like morphology with the length of 300 nm belongs to PDPP (Fig. 2a). Noticeably, the PDPP–GO composite material retains the lamellar structure of GO with the thickness of the clay flake increased (Fig. 2b), which is because PDPP evenly attached to the surface of GO from the enlarged view (Fig. 2c). Besides, it is worth noting that the size of PDPP in the composite has gone down compared with a pure substance. This is caused by the solvent effect of the PDPP crystalline compound. The chemical composition of the PDPP–GO was analysed by an energy dispersive spectrometer (Fig. S1†), and the spectrum clearly indicates the presence of C, N, and O elements. Additionally, the samples were tested using XRD to confirm the crystalline structure (Fig. 2d). For GO, a strong peak at 6.8° is ascribed to the characteristic peak of GO,[35] and a very tiny peak at 26° belongs to the characteristic peak of graphite.[36,37] In the curve of the composite material PDPP–GO, a strong and sharp peak can be observed at 10.8° of GO, illustrating the lamellar spacing of GO decreases. Meanwhile, the curve of PDPP–GO shows a new peak at 21.7°, which reveals that a few GO have been reduced to reduced graphene oxide (rGO). Moreover, the peak intensity was enhanced and the peak width became smaller, demonstrating that the PDPP molecules are spread over GO sheets. It also shows that the crystal structure of PDPP has changed and is completely consistent with the SEM. Besides, the surface area of PDPP–GO (22.033 m^2 g^{-1}, Fig. 2e) is 1.42 times that of GO (15.51 m^2 g^{-1}, Fig. 2f), which can profitably improve the electrocatalytic property. Raman spectroscopy also provides the structural information of the samples, as shown in Fig. S2,† the results show that the D band (1349 cm^{-1}) and G band (1602 cm^{-1}) of GO have no change in the peak position.

XPS analysis was used to further investigate the PDPP–GO composite material. As shown in Fig. 3a, the C 1s characteristic peaks of GO, respectively, are located at 284.8 eV (C=C/C–C), 286.6 eV (C–O), 287.3 eV (C=O), 288.6 eV (O–C=O),[38] and these

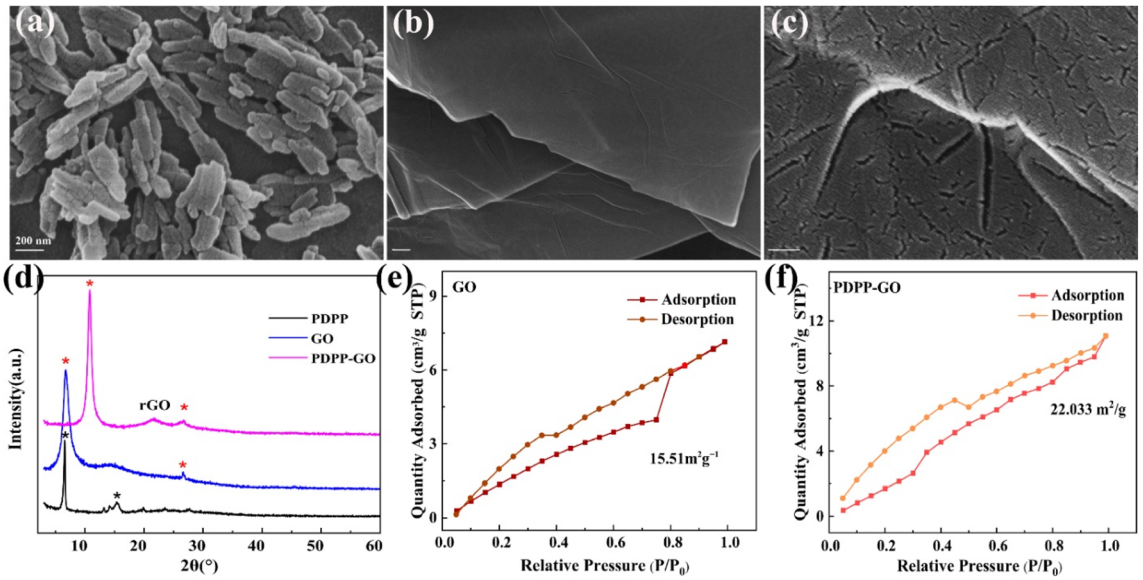

Fig. 2 SEM images of PDPP (a), PDPP–GO (b), and its enlarged view (c). (d) XRD pattern of samples. The special surface area of GO (e) and PDPP–GO (f).

peaks at 284.2 eV (C═C/C–C), 286.1 eV (C–O), 286.7 eV (C═O), 288.1 eV (O–C═O) belong to PDPP–GO. Remarkably, it must be added that all the binding energies of the PDPP–GO decrease by 0.5–0.6 eV with the binding form of carbon unchanged compared with the pure GO. Fig. 3b shows the high resolution of N 1s. Two obvious peaks at 398.8 and 400.1 eV correspond to C═N and NH of PDPP,[22,26] respectively. When PDPP combines with GO, the binding energies of the nitrogen move to higher energies 399.6 eV (C═N) and 401.3 eV (NH). The above results amply prove that π–π conjugation is generated between PDPP and GO molecules, which facilitated the electron cloud of PDPP transfer towards GO. Furthermore, what is particularly striking is that the binding energy of NH has a larger 1.2 eV difference value, demonstrating that the NH of PDPP and the OH of GO formed a hydrogen bond. These analysis results were further proved by the FT-IR spectra analysis.

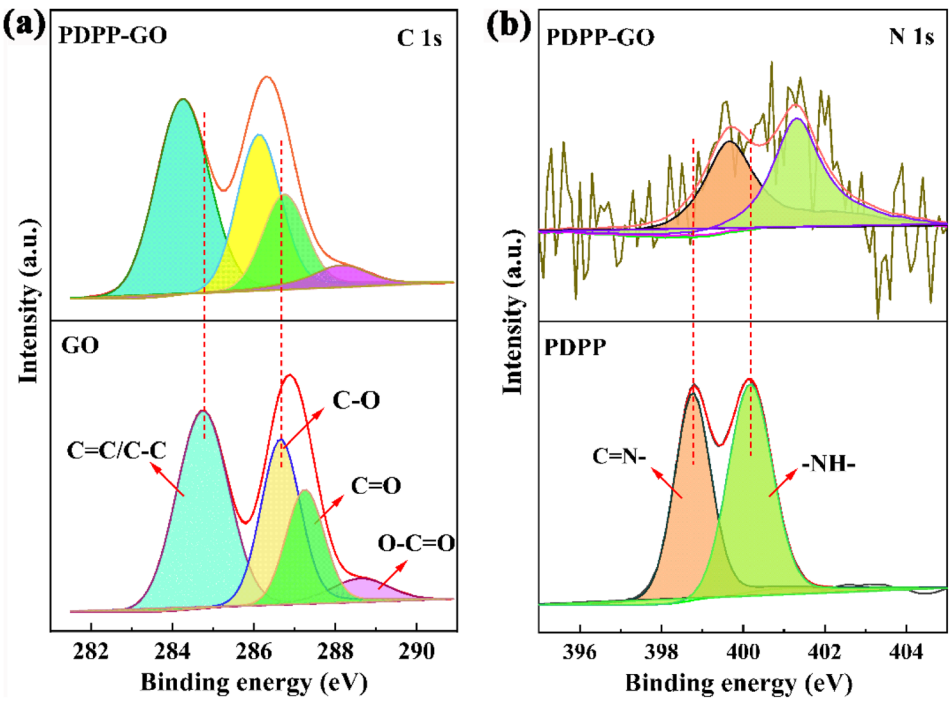

Fig. 3 XPS spectra of samples: high resolution of C 1s (a) and N 1s (b).

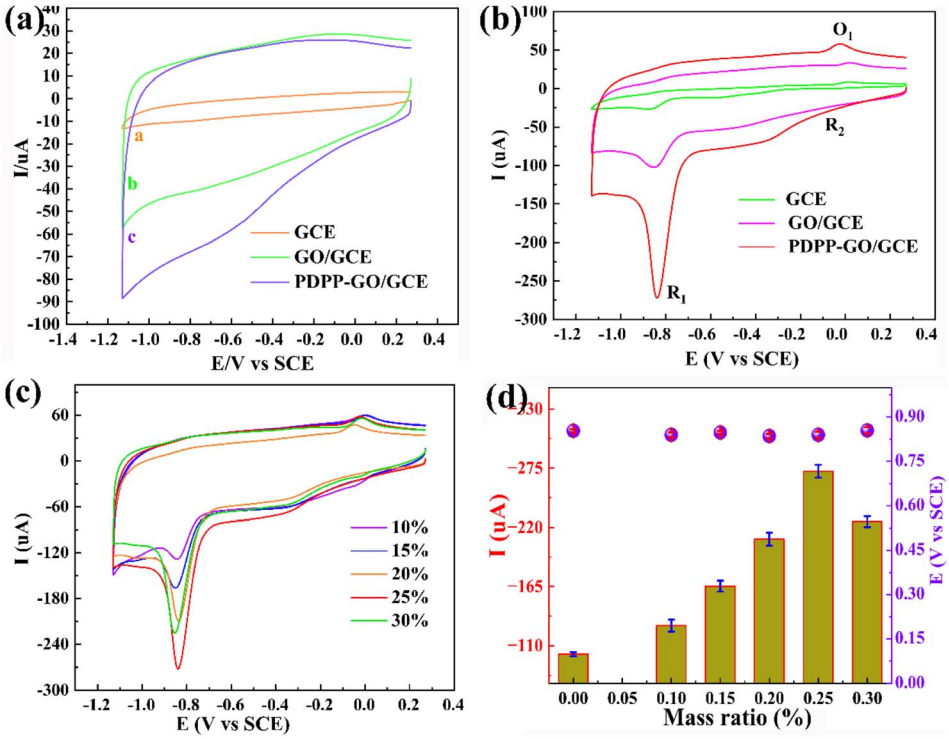

Fig. 4 CVs of bare GCE, GO/GCE, and PDPP–GO/GCE without (a) and with (b) 0.1 mM 4-NP in 0.2 M PBS (pH = 6.4), (c) CVs with different ratios of PDPP–GO composite material (wt%: 0%, 10%, 15%, 20%, 25%, 30%) with 0.1 mM 4-NP in 0.2 M PBS. (d) The plots of cathodic peak currents and potentials *vs.* mass ratio obtained from CVs. Scan rate: 50 mV s^{-1}. Potential window: 0.25 to −1.13 V.

3.2 Electrochemical behaviour of 4-NP at PDPP–GO/GCE

The direct electrocatalytic ability of the different modified electrodes towards 4-NP was investigated by cyclic voltammetry (CV) at a scan rate of 50 mV s^{-1}. Fig. 4a shows electrocatalytic activities of the obtained three electrodes (bare GCE, GO/GCE, and PDPP–GO/GCE) without 4-NP in 0.2 M PBS (pH = 6.4), and there were no characteristic peaks between 0.25 V and −1.13 V, which confirmed that these sensors are electro-inactive in the potential region and electrochemically stable. After adding 0.1 mM 4-NP (Fig. 4b), two reduction peaks R_1 (−0.87 V), R_2 (−0.02 V), and an oxidation peak O_1 (0.01 V) were observed in the CV curve of GCE, but all the peak current values are small. After GO and PDPP–GO modification of GCE, the reduction peak current (I_{pc}) of R_1 increases dramatically, and the peak current of R_2 and O_1 peaks remain virtually unchanged, hence the R_1 peak was used for sensitive detection of 4-NP. In the three above-mentioned electrodes, the PDPP–GO/GCE possesses the largest I_{pc} (−272 μA) at a more positive reduction potential of −0.84 V compared to others. These results demonstrated that PDPP enhanced the catalytic activity of GO to 4-NP, which is because the introduction of PDPP changes the electronic structure and morphology of the GO surface. The reduction peak R_1 at PDPP–GO/GCE revealed a four-electron transfer process to form 4-hydroxyaminophenol,[39,40] as shown in Fig. 5. The redox peaks at R_2 and O_1 correspond to the transformation between 4-hydroxyaminophenol and 4-nitroasophenol by two electrons.[41] Different mass ratios of PDPP–GO composite materials were also investigated by CV, as displayed in Fig. 4c. As the proportion of PDPP evolves from 0% to 30%, the reduction peak potential hardly moved, while 25% PDPP–GO/GCE exhibited the greatest I_{pc} (Fig. 4d). Hence, 25% PDPP–GO composite was used for subsequent studies.

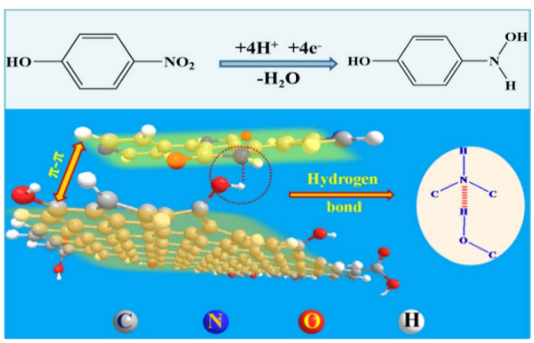

Fig. 5 Structure diagram and catalytic mechanism of PDPP–GO.

3.3 Effect of the scan rate and mechanism of the electrode reaction of 4-NP oxidation

The phenolic hydroxyl group of 4-NP is always involved in the electrochemical reaction, so it is quite necessary to investigate the pH value of the electrolyte. Fig. 6a shows the electrochemical redox behaviours of 0.1 mM 4-NP at the PDPP–GO/GCE at various pH (5.8, 6.0, 6.2, 6.4, 6.6, 6.8, 7.0) of 0.2 M PBS. It is evident that the reduction peak potential (E_{pc}) shifts

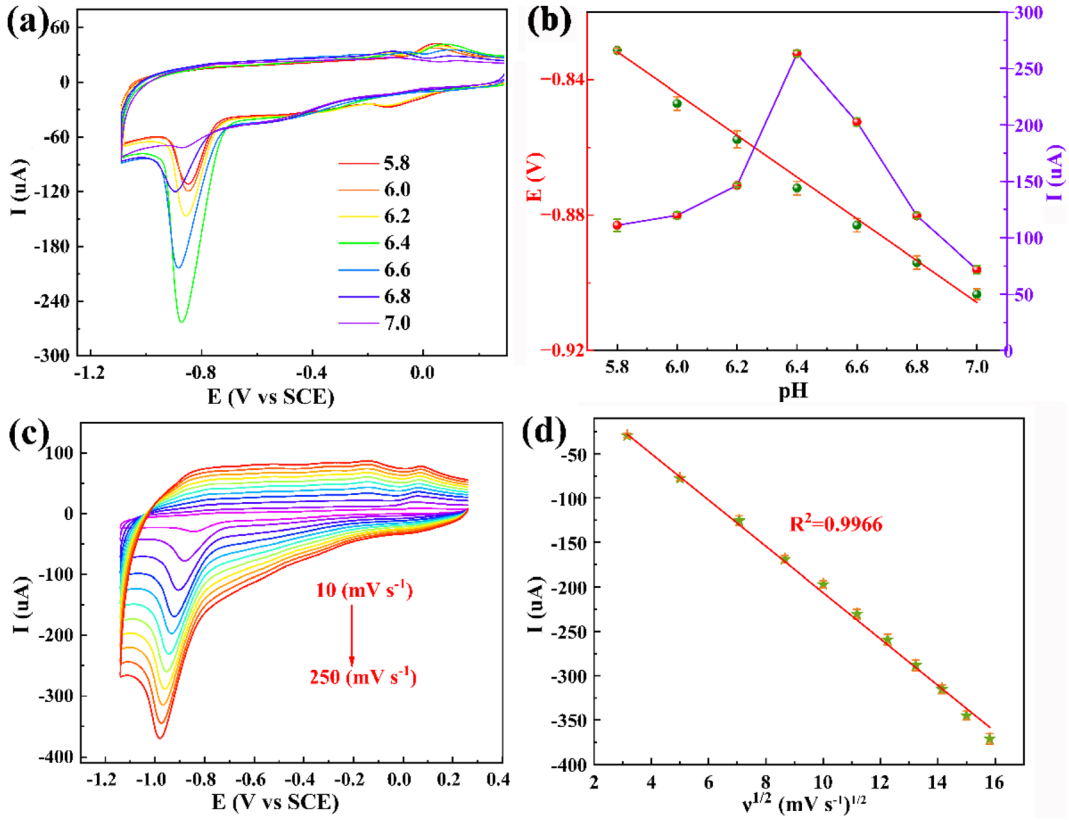

Fig. 6 (a) CVs of 0.1 mM 4-NP at PDPP–GO/GCE at various pH from 5.8 to 7.0, the scan rate is 50 mV s^{-1}; (b) linear relationship of E_{pc} *versus* pH value and the plot of I_{pc} *versus* pH value. (c) CVs of the PDPP–GO/GCE for 0.1 mM 4-NP in 0.2 M PBS at various scan rates: 10–250 mV s^{-1}, (d) the plots of cathodic peak currents *vs.* $v^{1/2}$. Potential window: 0.25–1.13 V.

negatively with pH increasing linearly, indicating that the proton participates in the electrochemical reaction of 4-NP. The linear relationship of E_{pc} *vs.* pH is clearly displayed by the linear regression eqn (2):

$$E_{pc}\ (V) = -0.0593pH - 0.490\ (R^2 = 0.9926) \quad (2)$$

According to the Nernst equation, the obtained slope value (0.0593 V pH^{-1}) is almost equal to the theoretical value (0.0591 V pH^{-1}), demonstrating that an equal number of proton and electron transfer were involved in the electrochemical reduction process of 4-NP. Moreover, the reduction catalytic current increases gradually from pH 5.8 to 6.4 and reach max at pH 6.4. When the pH value exceeded 6.4, the I_{pc} goes down (Fig. 6b). The results indicate that the optimal pH value for the 4-NP electrochemical reduction at PDPP–GO/GCE is 6.4.

The effect of the scan rate (v) on the peak current of 4-NP was also studied using CV with the scan rate changing from 10 to 250 mV s^{-1}. Fig. 6c shows the I_{pc} augments, stage by stage, and the E_{pc} moves to more negative. Applying the method of mathematical regression analysis of I_{pc} and scan rate, an excellent linear relationship is given on the basis of I_{pc} and the square root of the scan rate with regression eqn (3), as displayed in Fig. 6d.

$$I_{pc}\ (\mu A) = -26.64v^{1/2}\ (mV\ s^{-1})^{1/2} + 60.69\ (R^2 = 0.9966) \quad (3)$$

The obtained results clearly deduce that the electrochemical action of 4-NP at PDPP–GO/GCE belongs to the diffusion-controlled process.

3.4 Determination of 4-NP at PDPP–GO/GCE

In order to evaluate the electrochemical sensing capability of PDPP–GO/GCE, differential pulse voltammetry (DPV) was performed to measure I_{pc} under optimal conditions with a potential window of −0.6 to −1.05 V. The scan rate is 50 mV s^{-1}. It can be seen that the I_{pc} gradually becomes bigger with the 4-NP

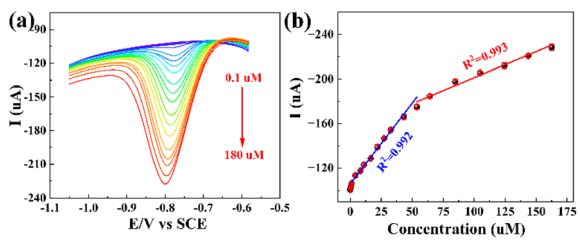

Fig. 7 (a) DPV curves of 4-NP with increasing concentration (0.1–180 μM) in 0.2 M PBS (pH = 6.4); (b) calibration plot of 4-NP *versus* concentration. Potential window: −0.6 to −1.05 V. Scan rate: 50 mV s^{-1}.

Table 1 Comparison of the electrocatalytic performance of different modified electrodes towards 4-nitrophenol detection

Electrode	Analytical method	Linear range (μM)	LOD (μM)	Sensitivity (μA μM^{-1} cm^{-2})	Ref.
SnO_2@ZIF-8/gC_3N_4	DPV	10–100	0.565	2.63	42
PSF/GCE	DPV	0.1–120	0.01		43
rGO/GCE	DPV	50–800	4.2	—	44
MMIPs/Au-NPs/AuE	DPV	0.1–1400	0.10	—	45
Fcc/hcp-Ni/GCE	CV	20–150	0.66	0.404	46
CTS/NPC/ITO	CV	50–400	27.55	4.85	47
rGO-HNT-AgNP/SPCE	DPV	0.1–364	0.048	35.25	17
PDPP–GO/GCE	DPV	0.5–163	0.10	18.54, 6.61	This work

concentration ranging from 0.1 to 180 μM (Fig. 7a), and two linear regression eqn (4) and (5) can be obtained from Fig. 7b.

$$I_{pc} = 1.310C_{4\text{-NP}} + 108.5\ (C_{4\text{-NP}}\text{: 0.5–50 μM},\ R^2 = 0.992) \quad (4)$$

$$I_{pc} = 0.467C_{4\text{-NP}} + 154.1\ (C_{4\text{-NP}}\text{: 50–163 μM},\ R^2 = 0.993) \quad (5)$$

The sensitivities of the PDPP–GO/GCE are 18.54 and 6.61 μA μM^{-1} cm^{-2}, respectively, by calculation, illustrating that the PDPP–GO/GCE executes more sensitively at low concentrations. When the PDPP–GO/GCE is exposed to a low concentration of 4-NP, the number of active sites is more than those required for 4-NP molecules; thus, 4-NP reacted completely and quickly. However, with the continuous increase of the concentration, the decreasing active sites compared to the total number of 4-NP molecules or absorbing oxidation product on the electrode surface led to the decrease of the second slope. The detection limit of 0.10 μM was calculated using the formula $3S/k$, in which k and S are the slope of the curve and the relative standard deviation of the blank solution. The results show that PDPP–GO/GCE could serve as an efficient 4-NP sensor with a wide detection range, low detection limit, and superior sensitivity. Table 1 displays the comparable 4-NP sensor, and the higher sensitivities of 18.54 and 6.61 μA μM^{-1} cm^{-2} emerge as focal points.

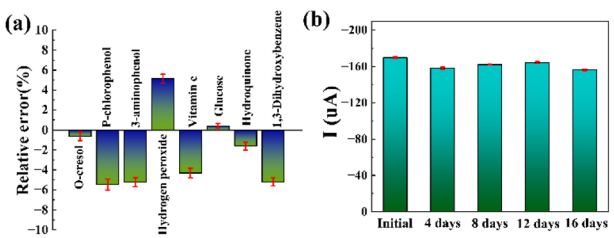

Fig. 8 (a) Selectivity of PDPP–GO/GCE containing 0.01 mM 4-NP in the presence of possible interfering compounds by DPV. The concentration of interferents was 0.25 mM. (b) Long-term stability of PDPP–GO/GCE toward 0.1 mM 4-NP at time intervals of four days at ambient conditions by DPV.

3.5 Interference, stability, and reproducibility

Interference, stability, and reproducibility are important static indicators for the electrochemical sensor. The interferences were performed in 0.2 M PBS containing 0.01 mM 4-NP in the presence of 0.25 mM of various possible interfering species, such as *o*-cresol, *p*-chlorophenol, 3-aminophenol, hydrogen peroxide, vitamin C, hydroquinone and 1,3-dihydroxybenzene. Fig. 8a shows the relative error of the I_{pc} after adding interferents and all data are less than ±5.5%, indicating these interferents have no significant effect on 4-NP detection. The PDPP–GO/GCE could be used for highly selective detection of 4-NP in the real sample. The stability of the PDPP–GO/GCE was estimated by intermittently measuring the current response of 0.1 mM 4-NP, and the current response remains 90% of its initial value over a storage period of 16 days (Fig. 8b), demonstrating the long-term stability of PDPP–GO/GCE. As for reproducibility, comparative analysis of the I_{pc} of five PDPP–GO/GCE, showed an excellent reproducibility with the relative standard deviation (RSD) of 2.52%, revealing the outstanding comprehensive performance of PDPP–GO/GCE to 4-NP.

3.6 Real sample analysis

The application of the PDPP–GO/GCE sensor for the detection of 4-NP was researched in tap water by the standard addition

Table 2 Recovery tests of 4-NP in tap water samples at PDPP–GO/GCE

Analyte	Samples	Detected[a] (μM)	Added (μM)	Found[a] (μM)	Recovery (%)	RSD (%)
4-NP	1	—	5	5.1 ± 0.11	102.0	2.2
	2	—	20	20.9 ± 0.13	104.5	0.6
	3	—	50	50.6 ± 0.45	101.2	0.9
	4	—	110	108.7 ± 1.23	98.8	1.1

[a] Mean value ± standard deviation for $n = 5$.

method, as shown in Table 2. Before testing, the tap water must be filtered to remove suspended materials. The test of the real water consisted of 2.00 mL filtered water and 8.00 mL 0.2 M PBS (pH = 6.4), and the DPV test showed that there was no signal for 4-NP. Therefore, 4-NP with different concentrations (5, 20, 50, 110 μM) were further analysed in the above solution. It is worth noting that the recoveries were between 98.8% and 104.5% with RSDs of 0.6–2.2%, exhibiting a sensitive and reliable determination for 4-NP using PDPP–GO/GCE in real samples.

4. Conclusions

In this work, a PDPP–GO composite material was synthesized by a simple method in an aqueous solution. Physical and chemical characterization results show that PDPP was tightly combined with GO by π–π stacking conjugation and strong hydrogen bonding. The advocated synthesis method simultaneously solved the electrical conductivity of GO and the solubility of PDPP, which opens up a new field for further construction with other materials in an aqueous solution. Notably, PDPP–GO/GCE shows excellent electrocatalytic activity for 4-NP detection with higher sensitivities of 18.54 and 6.61 $\mu A\ \mu M^{-1}\ cm^{-2}$ compared with other GO-based sensors. The PDPP–GO/GCE was proved for the detection of 4-NP in real samples and the comprehensive sensing performance of PDPP–GO/GCE perfectly meets the requirements for modern electrochemical sensors.

Author contributions

Lingpu Jia: formal analysis, conceptualization, methodology, investigation, validation, visualizations, writing – original draft, writing – review and editing. Shuangshuang Wang: software, investigation, formal analysis, methodology, resources. Long yang: writing – review and editing, methodology, investigation. Kunping Liu: writing – review and editing, supervision, project administration.

Conflicts of interest

There are no conflicts to declare.

Acknowledgements

This work was supported by the Second Tibetan Plateau Scientific Expedition and Research Program (STEP) (No. 2019QZKK0201), the National Natural Science Foundation of China (No. 22102134), The National Key Research and Development Program of Region innovation of Science and Technology Department of Sichuan Province (No. 2022YFQ0050) and the Introduction of Talent Research Start-up Fund of Chengdu University (No. 2081922036).

Notes and references

1 J. Xia, G. He, L. Zhang, X. Sun and X. Wang, Hydrogenation of nitrophenols catalyzed by carbon black-supported nickel nanoparticles under mild conditions, *Appl. Catal., B*, 2016, **180**, 408–415.

2 H. Yin, Y. Zhou, S. Ai, X. Liu, L. Zhu and L. Lu, Electrochemical oxidative determination of 4-nitrophenol based on a glassy carbon electrode modified with a hydroxyapatite nanopowder, *Microchim. Acta*, 2010, **169**(1–2), 87–92.

3 Z. Hasan, D.-W. Cho, C.-M. Chon, K. Yoon and H. Song, Reduction of p-nitrophenol by magnetic Co-carbon composites derived from metal organic frameworks, *Chem. Eng. J.*, 2016, **298**, 183–190.

4 S. Singh, N. Kumar, M. Kumar, A. Agarwal and B. Mizaikoff, Electrochemical sensing and remediation of 4-nitrophenol using bio-synthesized copper oxide nanoparticles, *Chem. Eng. J.*, 2017, **313**, 283–292.

5 X. Zhang, Y. S. Yang, Y. Lu, Y. J. Wen, P. P. Li and G. Zhang, Bioaugmented soil aquifer treatment for *p*-nitrophenol removal in wastewater unique for cold regions, *Water Res.*, 2018, **144**, 616–627.

6 D. Hofmann, F. Hartmann and H. Herrmann, Analysis of nitrophenols in cloud water with a miniaturized light-phase rotary perforator and HPLC-MS, *Anal. Bioanal. Chem.*, 2008, **391**(1), 161–169.

7 W. Zhu, Y. Zhou, S. Liu, M. Luo, J. Du, J. Fan, H. Xiong and H. Peng, A novel magnetic fluorescent molecularly imprinted sensor for highly selective and sensitive detection of 4-nitrophenol in food samples through a dual-recognition mechanism, *Food Chem.*, 2021, **348**, 129126.

8 F. Jaber, C. Schummer, J. Al Chami, P. Mirabel and M. Millet, Solid-phase microextraction and gas chromatography-mass spectrometry for analysis of phenols and nitrophenols in rainwater, as their t-butyldimethylsilyl derivatives, *Anal. Bioanal. Chem.*, 2007, **387**(7), 2527–2535.

9 H. F. S. AndreasGeiβler, Gaschromatographic determination of phenol, methylphenols, chlorophenols, nitrophenols and nitroquinones in water at 0.1 $\mu g\ L^{-1}$, *Water Res.*, 1994, **28**(10), 2047–2053.

10 X. Pang, H. Bai, Y. Zhao, L. Qu, D. Xu, J. Ding, W. Fan and W. Shi, Photoelectrochemical detection of 4-nitrophenol by sensitive Ni/Cu_2O photocathode, *Electrochim. Acta*, 2021, **367**, 137453.

11 S. Vinoth, P. Sampathkumar, K. Giribabu and A. Pandikumar, Ultrasonically assisted synthesis of barium stannate incorporated graphitic carbon nitride nanocomposite and its analytical performance in electrochemical sensing of 4-nitrophenol, *Ultrason. Sonochem.*, 2020, **62**, 104855.

12 Y. V. M. Reddy, J. H. Shin, V. N. Palakollu and et al, ., Strategies, advances, and challenges associated with the use of graphene-based nanocomposites for electrochemical biosensors, *Adv. Colloid Interface Sci.*, 2022, **304**, 102664.

13 J. P. Zou, Y. Chen, S. S. Liu, Q. J. Xing, W. H. Dong, X. B. Luo, W. L. Dai, X. Xiao, J. M. Luo and J. Crittenden, Electrochemical oxidation and advanced oxidation processes using a 3D hexagonal Co_3O_4 array anode for 4-nitrophenol decomposition coupled with simultaneous

CO_2 conversion to liquid fuels *via* a flower-like CuO cathode, *Water Res.*, 2019, **150**, 330–339.

14 K. Barman, B. Changmai and S. Jasimuddin, Electrochemical Detection of Para-nitrophenol using Copper Metal Nanoparticles Modified Gold Electrode, *Electroanalysis*, 2017, **29**(12), 2780–2787.

15 B. Khan, K. Akhtar, E. M. Bakhsh and A. M. Asiri, Electrochemical detection and catalytic removal of 4-nitrophenol using CeO_2-Cu_2O and CeO_2-Cu_2O/CH nanocomposites, *Appl. Surf. Sci.*, 2019, **492**, 726–735.

16 S. A. Hira, M. Nallal and K. H. Park, Fabrication of PdAg nanoparticle infused metal-organic framework for electrochemical and solution-chemical reduction and detection of toxic 4-nitrophenol, *Sens. Actuators, B*, 2019, **298**, 126861.

17 K.-Y. Hwa, T. S. K. Sharma and A. Ganguly, Design strategy of rGO–HNT–AgNPs based hybrid nanocomposite with enhanced performance for electrochemical detection of 4-nitrophenol, *Inorg. Chem. Front.*, 2020, **7**(10), 1981–1994.

18 J. Li, D. Kuang, Y. Feng, F. Zhang, Z. Xu and M. Liu, A graphene oxide-based electrochemical sensor for sensitive determination of 4-nitrophenol, *J. Hazard. Mater.*, 2012, **201–202**, 250–259.

19 C. Wang, Y. Yang, R. Li, D. Wu, Y. Qin and Y. Kong, Polyaniline functionalized reduced graphene oxide/carbon nanotube ternary nanocomposite as a supercapacitor electrode, *Chem. Commun.*, 2020, **56**(28), 4003–4006.

20 M. A. Auwalu and S. Cheng, Diketopyrrolopyrrole Fluorescent Probes, Photophysical and Biological Applications, *Chemosensors*, 2021, **9**(3), 44.

21 B. Sun, W. Hong, Z. Yan, H. Aziz and Y. Li, Record high electron mobility of 6.3 $cm^2\ V^{-1}\ s^{-1}$ achieved for polymer semiconductors using a new building block, *Adv. Mater.*, 2014, **26**(17), 2636–2642, 2613.

22 L. Yang, Y. Huang, Y. Peng, F. Liu, Q. Zhang, H. He, J. Wang, L. Jiang and Y. Zhou, Pyridine-Diketopyrrolopyrrole-Based Novel Metal-Free Visible-Light Organophotoredox Catalyst for Atom-Transfer Radical Polymerization, *J. Phys. Chem. A*, 2020, **124**(6), 1068–1075.

23 W. Li, A. Furlan, W. S. Roelofs, K. H. Hendriks, G. W. van Pruissen, M. M. Wienk and R. A. Janssen, Wide band gap diketopyrrolopyrrole-based conjugated polymers incorporating biphenyl units applied in polymer solar cells, *Chem. Commun.*, 2014, **50**(6), 679–681.

24 A. Tang, C. Zhan, J. Yao and E. Zhou, Design of Diketopyrrolopyrrole (DPP)-Based Small Molecules for Organic-Solar-Cell Applications, *Adv. Mater.*, 2017, **29**(2), 1600013.

25 J. W. Jung, F. Liu, T. P. Russell and W. H. Jo, Synthesis of pyridine-capped diketopyrrolopyrrole and its use as a building block of low band-gap polymers for efficient polymer solar cells, *Chem. Commun.*, 2013, **49**(76), 8495–8497.

26 L. Yang, Y. Yu, J. Feng, J. Wu, L. Jiang, Y. Dan and Y. Qiu, Charge transfer induced unexpected red-shift absorption of Zn and Cu porous coordination polymers based on electron-withdrawing ligand, *J. Photochem. Photobiol., A*, 2018, **350**, 103–110.

27 H. Bronstein, Z. Chen, R. S. Ashraf, W. Zhang, J. Du, J. R. Durrant, P. Shakya Tuladhar, K. Song, S. E. Watkins, Y. Geerts, M. M. Wienk, R. A. J. Janssen, T. Anthopoulos, H. Sirringhaus, M. Heeney and I. McCulloch, Thieno[3,2-*b*] thiophene-Diketopyrrolopyrrole-Containing Polymers for High-Performance Organic Field-Effect Transistors and Organic Photovoltaic Devices, *J. Am. Chem. Soc.*, 2011, **133**(10), 3272–3275.

28 C. Kanimozhi, N. Yaacobi-Gross, K. W. Chou, A. Amassian, T. D. Anthopoulos and S. Patil, Diketopyrrolopyrrole–Diketopyrrolopyrrole-Based Conjugated Copolymer for High-Mobility Organic Field-Effect Transistors, *J. Am. Chem. Soc.*, 2012, **134**(40), 16532–16535.

29 Z. Hao and A. Iqbal, Some aspects of organic pigments, *Chem. Soc. Rev.*, 1997, **26**, 203–213.

30 H. Lin, Z. Xu, L. Zhang, X. Yang, Q. Ju, L. Xue, J. Zhou, S. Zhuo and Y. Wu, Diketopyrrolopyrrole derivative functionalized graphene for high performance visible-light photodetectors, *New J. Chem.*, 2017, **41**(11), 4302–4307.

31 W. S. Hummers Jr, R. E. Offeman and W. S. Hummers, Preparation of graphitic oxide, *J. Am. Chem. Soc.*, 1958, **80**, 1339.

32 N. P. Shetti, L. V. Sampangi, R. N. Hegde and et al, ., Electrochemical oxidation of loop diuretic furosemide at gold electrode and its analytical applications, *Int. J. Electrochem. Sci.*, 2009, **4**, 104–121.

33 N. P. Shetti, S. J. Malode and S. T. Nandibewoor, Electro-oxidation of captopril at a gold electrode and its determination in pharmaceuticals and human fluids, *Anal. Methods*, 2015, **7**(20), 8673–8682.

34 K. Wu, H. Yang, L. Jia, Y. Pan, Y. Hao, K. Zhang, K. Du and G. Hu, Smart construction of 3D N-doped graphene honeycombs with $(NH_4)_2SO_4$ as a multifunctional template for Li-ion battery anode: "A choice that serves three purposes", *Green Chem.*, 2019, **21**(6), 1472–1483.

35 Y. Wei, X. Hu, Q. Jiang, Z. Sun, P. Wang, Y. Qiu and W. Liu, Influence of graphene oxide with different oxidation levels on the properties of epoxy composites, *Compos. Sci. Technol.*, 2018, **161**, 74–84.

36 L. Zhou, X. Lin, T. Huang and A. Yu, Binder-free phenyl sulfonated graphene/sulfur electrodes with excellent cyclability for lithium sulfur batteries, *J. Mater. Chem. A*, 2014, **2**(14), 5117–5123.

37 R. Ji, Q. Zhang, F. Zhou, F. Xu, X. Wang, C. Huang, Y. Zhu, H. Zhang, L. Sun, Y. Xia, X. Lin, H. Peng, Y. Zou and H. Chu, Electrospinning fabricated novel poly(ethylene glycol)/graphene oxide composite phase-change nanofibers with good shape stability for thermal regulation, *J. Energy Storage*, 2021, **40**, 102687.

38 C. Zhang, R. Hao, H. Liao and Y. Hou, Synthesis of amino-functionalized graphene as metal-free catalyst and exploration of the roles of various nitrogen states in oxygen reduction reaction, *Nano Energy*, 2013, **2**(1), 88–97.

39 A. D. Ambaye, K. K. Kefeni, T. G. Kebede and et al, ., Cu-MOF/N-doped GO nanocomposites modified screen-printed

carbon electrode towards detection of 4-nitrophenol, *J. Electroanal. Chem.*, 2022, **919**, 116542.

40 S. A. Hashemi, S. M. Mousavi, S. Bahrani and et al, ., Integrated polyaniline with graphene oxide-iron tungsten nitride nanoflakes as ultrasensitive electrochemical sensor for precise detection of 4-nitrophenol within aquatic media, *J. Electroanal. Chem.*, 2020, **873**, 114406.

41 J. Zhang, S. Cui, Y. Ding, X. Yang, K. Guo and J.-T. Zhao, Two-dimensional mesoporous $ZnCo_2O_4$ nanosheets as a novel electrocatalyst for detection of o-nitrophenol and p-nitrophenol, *Biosens. Bioelectron.*, 2018, **112**, 177–185.

42 D. Mohanta, A. Mahanta, S. R. Mishra, S. Jasimuddin and M. Ahmaruzzaman, Novel SnO_2@ZIF-8/gC_3N_4 nanohybrids for excellent electrochemical performance towards sensing of p-nitrophenol, *Environ. Res.*, 2021, **197**, 111077.

43 Y. Fang, D. Wang, X. Lv, X. Xu, H. Zhou, P. Liu, B. Cui and L. Wang, Simultaneous electrochemical determination of nitrophenol isomers based on spirofluorene - based microporous polymer film modified electrodes through one-step electropolymerization strategy, *Sens. Actuators, B*, 2021, **333**, 129568.

44 P. Wiench, B. Grzyb, Z. González, R. Menéndez, B. Handke and G. Gryglewicz, pH robust electrochemical detection of 4-nitrophenol on a reduced graphene oxide modified glassy carbon electrode, *J. Electroanal. Chem.*, 2017, **787**, 80–87.

45 G. Xu, L. Yang, M. Zhong, C. Li, X. Lu and X. Kan, Selective recognition and electrochemical detection of p-nitrophenol based on a macroporous imprinted polymer containing gold nanoparticles, *Microchim. Acta*, 2013, **180**(15–16), 1461–1469.

46 S. J. Lee, J. Theerthagiri and M. Y. Choi, Time-resolved dynamics of laser-induced cavitation bubbles during production of Ni nanoparticles *via* pulsed laser ablation in different solvents and their electrocatalytic activity for determination of toxic nitroaromatics, *Chem. Eng. J.*, 2022, **427**, 102687.

47 L. Hu, F. Peng, D. Xia, H. He, C. He, Z. Fang, J. Yang, S. Tian, V. K. Sharma and D. Shu, Carbohydrates-Derived Nitrogen-Doped Hierarchical Porous Carbon for Ultrasensitive Detection of 4-Nitrophenol, *ACS Sustainable Chem. Eng.*, 2018, **6**(12), 17391–17401.